On the Longitudinal Wave Pumping in Fluid-filled Compliant Tubes

On the Longitudinal Wave Pumping in Fluid-filled Compliant Tubes

Arian Aghilinejad,[1] Bryson Rogers,[1] Haojie Geng,[1] and Niema M. Pahlevan[1, 2]

[1)]*Department of Aerospace and Mechanical Engineering, University of Southern California, 1002 Childs Way, Los Angeles, CA 90089, USA*

[2)]*Division of Cardiovascular Medicine, Keck School of Medicine, University of Southern California, 1002 Childs Way, Los Angeles, CA 90089, USA*

(*Electronic mail: pahlevan@usc.edu)

(Dated: 9 August 2023)

This study investigates the physics of the longitudinal stretching-based wave pumping mechanism, a novel extension of the traditional impedance pump. In its simplest form, an impedance pump consists of a fluid-filled elastic tube connected to rigid tubes with a wave generator. These valveless pumps operate based on the principles of wave propagation in a fluid-filled compliant tube. Cardiovascular magnetic resonance imaging of the human circulatory system has shown substantial stretching of the aorta (the largest compliant artery of the body carrying blood) during the heart contraction and recoil of the aorta during the relaxation. Inspired by this dynamic mechanism, a comprehensive analysis of a longitudinal impedance pump is conducted in this study where waves are generated by stretching of the elastic wall and its recoil. We developed a fully coupled fluid-structure interaction computational model consisting of a straight fluid-filled elastic tube with longitudinal stretch at one end and fixed reflection site at the other end. The pump's behavior is quantified as a function of stretching frequency and tube wall characteristics. Our results indicate that stretch-related wave propagation and reflection can induce frequency-dependent pumping. Findings suggest a non-linear pattern for the mean flow-frequency relationship. Based on the analysis of the propagated waveforms, the underlying physical mechanism in the longitudinal impedance pump is discussed. It is shown that both the direction and magnitude of the net flow strongly depend on the wave characteristics. These findings provide a fundamental understanding of stretch-related wave pumping and can inform the future design of such pumps.

I. INTRODUCTION

Valveless impedance-based pumping is a promising technique for producing net flow with simple structure. In its conventional form, pumping is achieved via periodic radial compression of an elastic tube at an asymmetric location from the reflection sites[1–3]. The impedance mismatch, which is due to a connection in the tube of different compliances, creates wave reflection sites[2,4]. By compressing the elastic section periodically, traveling waves are emitted from the compression that can reflect at the impedance mismatches, generating a net flow[5,6]. While this pumping mechanism is first observed by Liebau[7], the first direct experimental evidence that this mechanism is involved in the nature is reported by Forouhar *et al.*[4]. This phenomenon has been well-investigated using analytical, computational, and experimental approaches that elucidate possible underlying mechanisms responsible for this phenomenon[8–13]. The conventional models mostly consist of fluid-filled elastic tubes in open and closed loops excited by a periodic total or partial compression of the tube[14]. Depending on wave parameters including the frequency, wave speed inside the tube and the location of the reflection sites, an impedance pump creates circulation of a fluid in a compliant tubing system in either direction[9,15,16].

Using a computational approach, Jung and Peskin[17] reported a strong non-linear dependence of the net flow on pinching frequency in the impedance pump. Later in a comprehensive experimental study, Hickerson, Rinderknecht, and Gharib[6] showed that the direction of flow is also dependent on the frequency of the compression. Their results also showed that the net pressure head and net flow as a function of the compression frequency had distinct peaks at selected frequencies[6]. Based on these findings, a one-dimensional wave model was proposed to predict the characteristics exhibited by the experiments[18]. Using this model, they showed the major role of wave reflection and interaction in the behavior of the impedance pump. More recently, Avrahami and Gharib[19] investigated the interplay of pressure, flow and elasticity in the impedance pump using a computational approach. They showed that pumping is the result of constructive wave interaction located at the extremity of the elastic tube distant to the pincher[19]. They also showed that the interaction location is very sensitive to the timing, and therefore to the frequency of excitation[19]. In another work, Loumes, Avrahami, and Gharib[20] showed that at resonance frequency, maximum energy transmission between the elastic tube and the fluid occurs and therefore, the elastic tube itself works as a pump which generates frequency dependent flow.

Besides the aforementioned studies, there have been efforts to extend the applicability of impedance pumping and introduce non-conventional impedance pumps. Carmigniani *et al.*[21] have recently developed a free-surface wave pumping mechanism where resonance pumping can be used for hydraulic energy harvesting. Similar to the conventional impedance pump, considerable bidirectional flow near certain frequencies was observed[21]. It was discussed that this type of impedance pump has strong application for renewable energy extraction. Anatol *et al.*[22] have recently implemented an actuator based on soft robotics technology in assymetric valvless pumping[23]. In 2006, Forouhar *et al.*[4] showed that the impedance-based pumping mechanism is involved in driving blood flow. Their findings suggested that in the embryonic heart tube, the role of the pincher is played by a band of active contractile cells near the heart entrance[4]. Several other stud-

ies have also shown the recurrence of the impedance pump mechanism in biological systems[24]. Pahlevan and Gharib[25] showed the similar pumping behavior to impedance pump in the human aorta. The difference between an aortic pump and an impedance pump is that there is no external pincher in the aortic wave pumping mechanism; rather, the flow waves are generated by the heart and the aorta works as a fluid-filled elastic tube with multiple reflection sites. This aortic wave pumping effect can generate a bidirectional flow depending on the state of the wave dynamics[25].

While the impedance pumping system can serve as an energy-efficient and simple flow generators, there are technical challenges that limits the applicability of such devices[1,14]. The low mean flow rates seen in the previous studies are troublesome since they offer a little use for real flow improvement especially in physiologically relevant settings[26]. In addition, there are disagreements on the optimal performing condition of conventional impedance pumps due to the complexity in their characteristic behavior[6,27]. In this study, we present a novel extension of impedance wave pumping based on the longitudinal stretching of a compliant tube. This wave pumping mechanism is inspired by the longitudinal stretch of the ascending aorta (the largest compliant artery of the body that carries blood from the heart) in the cardiovascular system. In an optimal left ventricle-aorta coupling, the left ventricular systolic contraction displaces the aortic annulus and produces a considerable longitudinal stretch of the ascending aorta[28]. This longitudinal (axial) displacement results in energy storage in the vessel's spring-like elements that enhances early diastolic left ventricle recoil and creates suction in the heart that facilitates diastolic filling[29,30]. Longitudinal stretching of the ascending aorta during the contraction of the left ventricle has been recognized by the medical community as an important determinant of aortic biodynamics[29,31]. However, this dynamic mechanism has not been investigated in the context of wave pumping in the complaint tubes. Understanding such pumping can provide better insights on the role of aorta in transferring blood inside the body and potentially be useful in designing assist devices for patients suffering from reduced cardiac output.

Our central hypothesis is that stretch-related wave propagation and reflection in a fluid-filled compliant tube, inspired by the aortic natural mechanism, can create a wave pumping mechanism. This longitudinal wave pumping and the conventional impedance pumping differ in their wave generating system, but both pumping mechanisms rely on the principles of wave propagations and reflections. To understand the underlying mechanism in the longitudinal stretching-based impedance pump, we employ a computational approach of a fluid-filled elastic tube with fluid-structure interaction modeling. The pump's behavior is characterized as a function of various stretching parameters as well as different wave characteristics. Generally, wave dynamics in a compliant tube are dominated by three parameters: 1) the fundamental frequency of the propagating waves, 2) wave speed, which is determined by the material property of the medium, and 3) the locations of reflection sites[4,19,32]. In this study, we investigate the impact of these parameters in the context of the longitudinal

impedance pump. First, we investigate the frequency dependency of the net generated flow by imposing different stretching frequencies on the longitudinal displacement profile of the tube root. Simulations are also conducted for different levels of tube stiffness to investigate the effect of the wave speed on the longitudinal pumping. Lastly, different tube lengths are considered to assess the effect of reflection site location on the wave pumping mechanism. The findings from this study provide insights on the working principle of the longitudinal impedance pump and can guide and optimize the design of such pumps for future use.

II. MATERIALS AND METHODS

A. Physical problem

The physical problem of interest consisted of a straight cylindrical tube filled with water, with one end fixed and the other stretched cyclically at frequency f (Fig. 1). In this figure, r_f is the radius of the fluid domain, r_s is the radius of the solid domain, and the difference of the two is the wall thickness (t_s). L in this figure represents the length of the tube. The cylindrical coordinate system is also employed with radial component r, azimuth ϕ, and axial component z. Each period of the cyclic extension consisted of two phases: stretching and recoil. The elastic wall of the pump is first stretched to a distance, then released during the recoil phase. The recoil is passive, meaning it is only due to the elasticity of the tube wall. The elastic recoil results in wave propagation along the wall with initial amplitude D_w which is reflected upon reaching the fixed outlet. Since our investigation is inspired by the human aorta, baseline parameters were selected within the average physiological ranges[33–36]. The fluid in this study is assumed to be Newtonian[37–41]. The parameters used in this study are summarized in Table I.

B. Governing equations

Fluid motion is computed using the continuity and conservation of momentum equations of an incompressible fluid given by

$$\nabla \cdot \boldsymbol{v} = 0 \tag{1}$$

$$\rho_f \dot{\boldsymbol{v}} + \rho_f \left(\boldsymbol{v} \cdot \nabla \right) \boldsymbol{v} - \nabla \cdot \boldsymbol{T}_f - \boldsymbol{f} = 0, \tag{2}$$

TABLE I. Physical parameters used in the model.

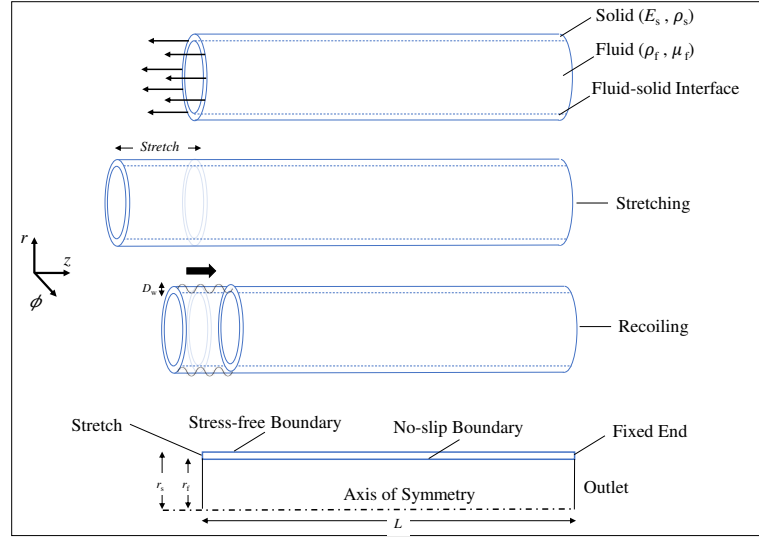| Physical Parameter	Symbol	Value
Solid wall thickness (m)	t_s	0.001
Solid wall density (kg/m^3)	ρ_s	1050
Poisson ratio of the solid wall	υ_s	0.45
Fluid density (kg/m^3)	ρ_f	1050
Fluid viscosity (Pa.s)	μ_f	0.005
Fluid domain radius (m)	r_f	0.015

FIG. 1. Schematic representation of the longitudinal impedance pump. Different phases during one cycle are shown. An illustrative sketch of the axisymmetric model and the computational boundaries are also shown. E_s and ρ_s are the module of elasticity and the density of the solid wall, and ρ_f and μ_f are the density and viscosity of the fluid, respectively. r_s and r_f are the radius of the solid and fluid domains, respectively. L is the length of the tube. $r = 0$ line is located at the root of the tube.

$$T_f = -pI + \mu(\nabla v + \nabla v^T), \qquad (3)$$

where v is fluid velocity, ρ_f is fluid density, T_f is the fluid stress tensor (for the Newtonian and incompressible fluid), f is body force, p is pressure, I is the identity tensor, and μ is the fluid dynamic viscosity in Eq. 1 to 3. Motion of the linearly elastic vessel wall is calculated using the Lagrangian form of the momentum balance equation (Eq. 4) given by

$$\frac{\partial T_s}{\partial X} + F = \rho_s \ddot{u}_s, \qquad (4)$$

where X is the position of a material point, T_s is the solid stress tensor (considered as a linear elastic material), F is the vector of external force, ρ_s is vessel wall density, and $\ddot{u}_s$ is wall acceleration. At the fluid-structure interface the fluid is fully coupled to the solid. The conditions applied to the fluid-structure interface are displacement compatibility and traction equilibrium between the two surfaces (Eq. 5 and 6). Applying a no slip boundary condition at this interface, the fluid-structure coupling conditions are given by

$$r = r_f : \quad v = \dot{u}, \qquad (5)$$

$$r = r_f : \quad n \cdot T_f = n \cdot T_s, \qquad (6)$$

where $\dot{u}$ is the solid velocity, and n is the normal vector of the fluid-solid interface in Eq. 6. To ensure total wave reflection, outlet of the vessel was fixed (Eq. 7), such that

$$u = 0, \qquad at \qquad z = L \qquad (7)$$

C. Description of the boundary conditions

In the fluid domain, zero pressure is applied to the inlet and outlet while an axisymmetric boundary condition was applied to the inner edge ($r = 0$). At the interface of the fluid and solid domains, no slip boundary condition is applied (Eq. 5 and Eq. 6). In the solid domain, zero traction ($T_s = 0$) is applied to the outer edge ($r_s = r_f + t_s$), and the inlet edge is extended cyclically using a custom hybrid boundary condition. One cycle of the boundary condition consists of a stretching and a recoil. During stretching, a prescribed velocity profile is applied to the wall to elongate the tube. The shape of the velocity waveform is taken from the root displacement measurements of the aorta using cardiovascular magnetic resonance by Codreanu *et al.*[31]. Data are adopted from their measurements and then polynomial curve is fitted on the measurements using Matlab (MathWorks 2022). For the beginning of the cycle, a linear profile is applied since there was no reported clinical measurement. Fig. 2 demonstrates their reported data overlaid by the prescribed velocity profile used in this study during the stretching phase (T_{stretch}). The maximum amount of stretch is determined by computing the area under the velocity-time curve and normalized by the length of the tube (stretching coefficient, SR). Recoil begins after peak displacement is reached, when the prescribed velocity is replaced by a zero-traction boundary condition and the tube relaxes due to its own elasticity. The summation of the stretching and recoil phases complete one period. To control the length of the

Accepted to Phys. Fluids 10.1063/5.0165150

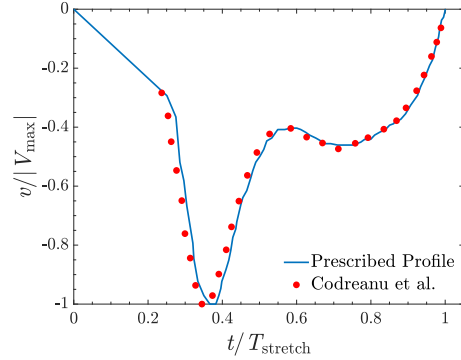On the Longitudinal Wave Pumping in Fluid-filled Compliant Tubes 4

FIG. 2. Implemented boundary condition at the tube root based on the reported physiological measurement. The prescribed velocity profile applied to the root wall during the stretching phase overlaid on top of the reported magnetic resonance measurements done by Codreanu *et al.* [31].

Algorithm of Longitudinal Wave Pumping System Model.

Input: fluid-filled elastic tube model L, r_f, t_s, E_s, μ_f, ρ_f, ρ_s, ν_s

Input: boundary parameters SR, f, duty cycle (DC)

Input: discretization (Δt) and number of cycles to simulate ($\Rightarrow$ final time t_f)

Initialize: solid and fluid domains with zero velocity and stress

1   while $t < t_f$ do
2   if ($\text{mode}(t,T) < DC$) then   // $T \leftarrow \frac{1}{f}$
3   prescribe velocity profile to the tube root   // active stretching (Fig. 2)
4   else
5   zero traction to the tube root   // passive recoil
6   end
7   solve for fluid pressure and velocity fields at $t + \Delta t$ // via Eq. (1) and (2)
8   prescribe the fluid forces at the fluid-structure interface   // via Eq. (3)
9   solve for solid displacement and stress fields at $t + \Delta t$ // via Eq. (4)
10   apply no-slip condition at the fluid-solid interface, $t \leftarrow t + \Delta t$ // via Eq. (5) and (6)
11 end

Output: Numerical solutions for $v(x,t)$, $p(x,t)$ and $u(X,t)$ on $[0,t_f]$

FIG. 3. Description of fluid-structure interaction algorithm to solve the longitudinal wave pumping system model.

stretching phase, the duty cycle (DC) is defined which is the ratio of the stretching time over the full cycle. (DC) is fixed to $1/3$ in this study which is inspired by the systolic time over the full period.

D.   Computational model and numerical method

The 2D axisymmetric model in this study consists of a fluid domain and a solid domain coupled at the inner edge of the tube wall. For solving the fluid and solid domains numerically, we use the finite element method. The fluid-structure interaction model employs the Arbitrary Lagrangian-Eulerian method. This method uses a generalized explicit numerical formulation and capture the advantages of both Eulerian and Lagrangian methods for simulating the large deformation problems [42,43]. Therefore, this approach is suitable for investigating the wave pumping in the longitudinal impedance pump with considerable stretch at the root of the tube [19,20]. The inputs, algorithm, and outputs of the computational model are summarized as a pseudo-code in Fig. 3. The output of the numerical solver is the fluid velocity ($v(x, t)$), fluid pressure ($p(x, t)$), and solid displacement ($u(X, t)$). The system is initialized at rest, with zero pressure and velocity in the fluid, and zero stress and strain in the solid. The fluid and solid domains consist of 1040 and 260 elements, respectively, and the time step is 0.001s. Appendix A presents our sample results for the spatial and temporal discretization-independence studies. Note that these numbers were obtained for the largest tube length used in this study (i.e., $L = 50$cm). The period of the cycle is determined by f and the relative durations of the stretching and recoil were determined by duty cycle (DC). A computational model of the physical problem is generated and solved using the finite element solver ADINA version 9.7 (ADINA R&D Inc., MA). Simulations are run on a standalone

workstation equipped with an Intel Core i7 CPU (6 cores and 3201 MHz) with 32GB memory. At least 35 cardiac cycles were simulated for each case to ensure a periodic steady state is reached. Appendix B provides the details for the definition of periodic steady-state used in this study. The inputs, algorithm, and outputs of the computational model are summarized as a pseudo-code in Fig. 3.

E.   Analysis method

Wave dynamics in an elastic tube depends on three major parameters: *i)* frequency of the wave generator, *ii)* wave speed, and *iii)* reflection sites [4,33,44]. In the first step, the natural frequency of the system is computed using the developed computational model. A free vibration test and a spectral analysis are carried out to identify the natural frequencies. To perform the free vibration test, the tube model is stretched using a step-function and immediately released, continuing until both fluid and solid motion ends. The propagating waves are then analyzed using their corresponding power spectra. In this analysis, the proportion of the total signal power contributed by each frequency component is determined from the discrete Fourier transform (via FFT). The squared amplitude, averaged by the number of samples, is then computed for each frequency component. The relation between the natural frequency and the wave speed in a fluid-filled elastic tube can also be calculated from the empirically-derived formula [14]

$$f_n = n\frac{c}{2L}, \tag{8}$$

where f_n is the natural frequency of the system corresponding to the nth harmonic, c is the speed at which the waves propagate in the tube (wave speed), and L is tube length. To compute the wave speed, we utilized the Moens-Korteweg equa-

TABLE II. Parameter settings for different case studies.

Physical Parameter	Symbol	Range
Length of the tube (m)	L	[0.125, 0.50]
Wall elasticity (kPa)	E_s	[100, 900]
Stretching over length ratio	SR	[0.04, 0.10]
Stretching frequency (Hz)	f	[0.5, 4]

tion given by,

$$c = \sqrt{\frac{E_s t_s}{2 r_f \rho_f}}, \qquad (9)$$

where E_s is the Young modulus of the wall, t_s is the wall thickness, r_f is the internal radius, and ρ is the fluid density. We compared the computed natural frequencies using Eq. 8 and the ones from the computational model. Simulations are run for different levels of tube stiffness which is quantified by the wave speed inside the tube (Eq. 9). At each wave speed, the simulations are done for 9 different frequencies (0.5, 0.8, 1, 1.25, 1.6, 2, 2.5, 3.2, and 4 Hz). The simulations are also run for different tube lengths. Ranges of the parameters employed in the simulations are listed in Table II. The range of the utilized parameters are inspired by the human cardiovascular system and they fully covered the physiological condition[35,36,45,46]. In this table, SR is defined as the stretch ratio which is amplitude of the maximum stretch scaled by the initial tube length.

III. RESULTS AND DISCUSSION

A. Wave speed and natural frequency

Given the baseline characteristic in our model ($L = 0.5$m, $r = 0.015$m, $E_s = 100$KPa, density of $1050\ kg/\text{m}^3$, and thickness of 0.1cm), Eq. 9 yields $c = 1.78$m/s. Therefore, the first three expected natural frequencies for this model, computed by Eq. 8, are $f_1 = 1.78$Hz, $f_2 = 3.56$Hz, and $f_3 = 5.34$Hz. Fig. 4(a) shows the computed displacement of the root (inlet) for a free-vibration test with stretching coefficient of $SR = 0.1$, which corresponds to 5cm stretch for 50 cm tube length. The displacement of the root is sampled for 10s, beyond which the amplitude of the displacement is nearly zero. A Fast Fourier Transform (FFT) was applied to identify the model's natural frequencies, shown in Fig. 4(b). The computed natural frequencies match well with the theoretical values. This comparison shows that the employed fluid-structure interaction modeling (Fig. 3) is capable of capturing the wave dynamics accurately.

B. Effect of the stretching frequency

Figures 5(a, b) depict the root displacement and outlet flow profile during one oscillatory steady-state period (T) at different frequencies. In order to investigate the effect of the stretching frequency, we fixed the applied profile to the tube root (Fig. 2), and changed the length of the cycle. By fixing the tube length and the wave speed, we tracked the relation between the outlet flow profile and the excitation frequency. The displacement profile during the stretching phase is due to the applied boundary condition to the wall and therefore, for different frequencies it has a similar shape. As the recoil starts, the displacement-time variation exhibits the characteristics of a mass-spring system reacting to an initial force with an overshoot and subsequent oscillations. The exact response of the tube and the oscillation at the root varies across different frequencies. Like conventional impedance pump, as the excitation happens, the waves are allowed to travel along the tube and are then partially reflected at the outlet interface. As the frequency changes, even for the same wave speed and tube length (fixed travel time), the interactions between the forward running waves and the reflected ones changes. In Fig. 5(b) outlet flow is computed by integrating fluid velocity across the outlet elements. Similar to the displacement profile, the flow profile varies dramatically across different frequencies in terms of both amplitude and direction.

Fig. 6(a) presents mean outlet flow $\bar{Q}$ obtained via averaging the flow over one period T as a function of frequency. The mean flow-frequency data in this plot are obtained at the given baseline parameters for the model ($L = 0.5$m, $r = 0.015$m, $E_s = 100$KPa, density of $1050 kg/\text{m}^3$, and thickness of 0.001m). The mean outlet flow $\bar{Q}$ is an indicator of the bulk flow motion for the specific wave condition. The data presented in Fig. 6(a) suggest a non-linear mean flow-frequency relationship similar to the previously-observed trends in the experimental and computational studies of the conventional impedance pumps[6,18,19,25]. The dominant negative flow (toward stretched and excited inlet) reported in Fig. 6(a) suggests the significant the impact of the suction created during the stretching phase. However, there are certain frequencies which affect the flow direction and cause positive net flow generation (toward the fixed outlet). The frequency spectra of oscillatory part of the outlet flow obtained by FFT at three sample frequencies, where the flow pattern changes, are plotted in Fig. 6(b, c, d). Results suggest that for the case with negative net flow (reverse pumping mode), the first harmonic is dominant while for the positive cases (pumping mode) the second mode is dominant. The transition between the modes is due to the change in the wave state which is a result of wave propagation and reflection. Previous studies have shown that the net effect of the incident and reflected waves in a fluid-filled elastic tube is a function of the excitation frequency[47]. It has been shown that the tube impedance (which is defined based on the pressure and flow harmonics) get minimized at certain frequencies close to the one-quarter wavelength frequency ($\hat{f}_1 = c/\lambda_1$ given $\lambda_1 = 4L$) and three-quarter wavelength frequency ($\hat{f}_2 = c/\lambda_2$ given $\lambda_2 = 4L/3$)[47]. The strong dependency of the generated flow profile to the applied frequency here is hence due to the superposition of the propagating waves created due to the longitudinal stretch and reflected ones at the tube outlet. Results from Fig. 6 suggests that at certain frequencies (e.g., 1Hz or 2.5Hz), the generated positive flow due to the interference of the traveling and reflected
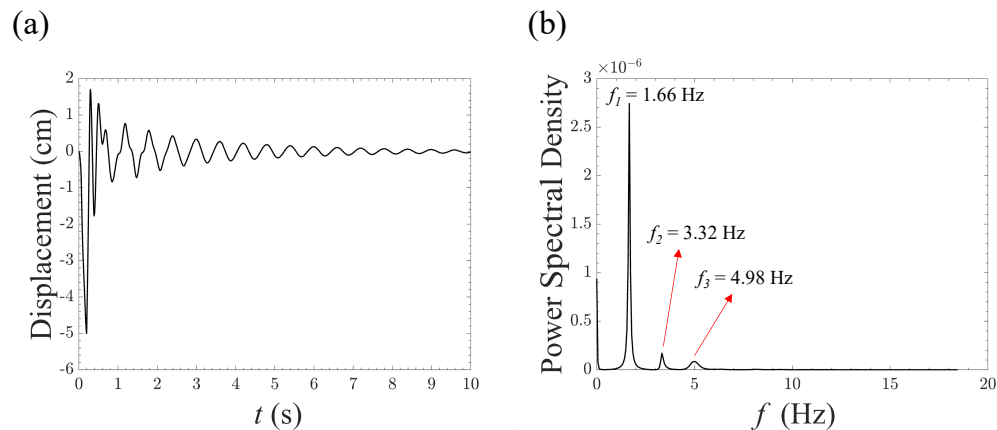
(a)

(b)

FIG. 4. System's response to impulse stretching. (*a*) The transient response of longitudinal component of the wall displacement, and (*b*) the power spectrum density of the outlet flow signal. The peaks correspond to the natural frequencies of the system. The corresponding theoretical values are 1.78Hz, 3.56Hz, and 5.34Hz for the first three natural frequencies respectively.

waves at the outlet dominate the negative flow generated by the suction (due to the stretch itself) and hence, the net flow is positive. In other words, these frequencies alter exisiting trend in the longitudinal impedance pump, leading to a non-linear mean flow-frequency relationship.

C. Driving mechanism in the longitudinal impedance pump

Conventional impedance pumps operate based on the pressure wave generation by the periodic tube wall excitation[14,18,19]. It is shown in some studies that for achieving the maximum pressure difference to generate flow, the system has to be excited close to its natural resonant frequencies[19]. However, there are some other studies that reported significant generated flow at frequencies far below the natural frequency[14]. Either way, the unique frequency dependence of the net flow rate implies a wave-driven flow[6]. Our findings indicate that there are two modes in the longitudinal impedance pump, the reverse pumping mode and the pumping mode. Our results suggest that there is a mode transition between the reverse pumping and the pumping mode, where in the former one the first harmonic corresponding to the stretching frequency is dominant and in the latter one the second harmonic is dominant (Fig. 6). Similar mode transition has been previously reported by Kim *et al.*[48] for the flexible ring immersed in the fluid. From the frequency spectra, two modes were identified in their study; the energetic mode where the first harmonic is dominant and ordinary mode where the second harmonics is dominant. The energetic mode corresponds to the flapping motion and the ordinary mode corresponds to the elastic vibrations[48,49]. Fig. 7 presents the radial displacement profiles of the tube wall at given frequencies. These plots

suggest that there are two patterns for the wall displacement depending on the excitation frequency; the energetic mode which leads to the flapping motion at frequencies of 0.8 and 1.6Hz (the first harmonic is dominant) and the ordinary mode which leads to the elastic oscillations at frequencies of 1.0 and 2.5Hz (the second harmonic is dominant as shown in Fig. 6). The flapping motion is attributed to the large displacement in the tube wall (as shown in Fig. 7) while elastic oscillation is attributed to the smaller displacements. For the ordinary mode, it can be noticed that the interactions of the propagated and the reflected wave yields a lower amplitude wave on the tube wall. On the other hand, the amplitude of the tube wall displacement for the energetic mode is more significant.

Fig. 8 presents distributions of the fluid pressure at various snapshots in time during one cycle. The longitudinal impedance pump demonstrates both positive flow generation (pumping) and negative flow generation (reverse pumping) based on the stretching frequency. In the negative flow cases, as the pressure drops due to the stretching, a flow begins to fill the low-pressure region (stretched portion of the tube) from a higher-pressure region (resting portion of the tube). By modifying the stretching frequency and fixing the travel time (constant tube length and wave speed), a coordination between the propagated and reflected waves can be achieved such that net unidirectional flow is sustained. The stretching of the tube results in a suction as demonstrated in Fig. 8. During recoil, the flow generation is determined primarily by the compression reflected pressure waves. The net pressure distribution inside the tube which ultimately determines the flow propagation is dictated by the initial suction due to the stretching and the wall displacement determined by the wave state. Depending on having either the energetic or ordinary mode, the response of the wall changes which consequently changes the pressure
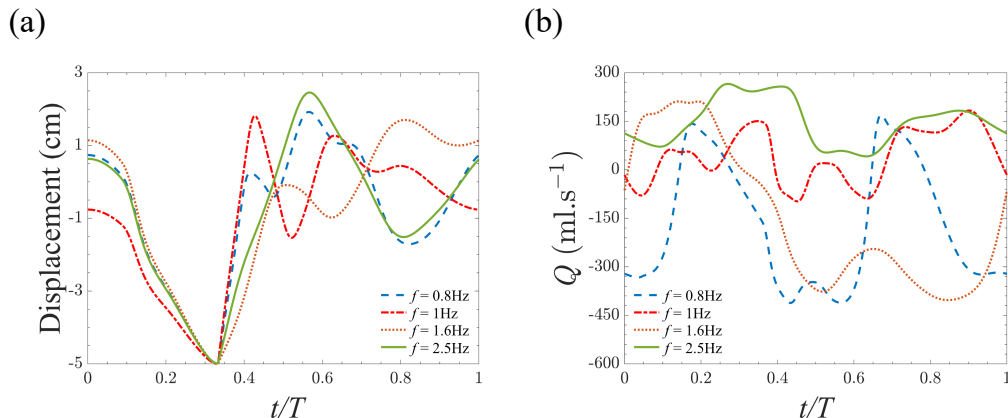
Accepted to Phys. Fluids 10.1063/5.0165150

On the Longitudinal Wave Pumping in Fluid-filled Compliant Tubes 7

(a)

(b)

FIG. 5. Sample displacement waveforms at the root and flow waveforms at the outlet. (*a*) Root (inlet) displacement and (*b*) outlet flow at given different excitation frequencies.

and flow distributions.

As an example of the impact of the tube wall displacement on the pressure and flow relationship, we presented the $P - Q$ loop during an oscillatory steady-state cycles at different locations along the tube in Fig. 9. The data presented in this figure show that loop direction tends to flip once along the length of the tube. Near the inlet where the stretching occurs, the elastic wall does work on the fluid, and the $P - Q$ loop is thus counterclockwise. Closer to the outlet, the interaction of the suction and compression waves impedes flow, resulting in work done by the fluid on the walls and clockwise $P - Q$ loop. These sampled data are collected for frequency of 1.6Hz. To examine the effect of frequency on the pressure and flow relationship, we presented the power expenditure, computed form the loop areas of the P-Q curves, as a function of axial location along the tube for three representative frequencies in Fig. 15 (Appendix C). Results suggest that changing the frequency mostly affect the amplitude of the area inside the P-Q loop at different locations and does not alter the overall pattern.

D. Effect of the stretching amplitude

To further investigate the underlying mechanism associated with longitudinal wave pumping, the stretching amplitude is varied. Sample longitudinal displacement and the pressure collected near the outlet (5cm away of the outlet) are plotted in Fig. 10. These plots are demonstrated for different stretching amplitudes and frequencies. Results suggest that increasing the stretching amplitude elevate the pressure gradient at each fixed frequency. However, increasing the frequency alone at fixed stretching amplitude does not necessarily lead to the elevation in the pressure. For example, increasing the frequency from 0.8Hz to 1.0Hz decrease the pressure amplification while

further increase from 1.0Hz to 1.6Hz lead to an increase in the pressure amplification. The similar non-linear dependency can also be observed in the displacement profile. The stretching amplitude is one of the major determinants of the input power to the longitudinal impedance pump. The elastic wall can be assumed as a spring where the displacement results in energy storage in the elastic wall elements. This input energy has linear relation with the stretch. Since the net generated flow and the pressure gradient by the wave pumping mechanism are related to the power (or energy) carried by the waves[25], the stretching amplitude elevates the pressure gradient consistently. On the other hand, as shown in Fig. 6 and Fig. 9, the effect of the frequency on the net generated flow (which is created due to the pressure gradient) is non-linear and depends on the mode of excitation (energetic mode vs ordinary mode).

Fig. 11 presents the flow as a function for the applied stretching frequency in the longitudinal impedance pump model for stretching of 2cm ($SR = 0.04$), 2.5cm ($SR = 0.05$), 3.7cm ($SR = 0.74$), and 4.3cm ($SR = 8.6$). The power spectra for the outlet flow at the local positive and negative peaks for all cases are also demonstrated in these plots. Similar to the findings from Fig. 6, results suggest that the second harmonic is dominant for the pumping mode, while the first harmonic is dominant in the reverse pumping mode. The transition in the dominant mode in the flow waveform yield a resonance-like behavior in the mean flow-frequency pattern, where the initial negative value for the flow (which is due to the stretching-based suction at the inlet) varies to the positive values. At the given stretching amplitude, the positive flow pumping is due to the wave dynamics on the wall in its ordinary mode which lead to the elastic oscillations. Results also suggest that the amplitude of the stretch does not change this pattern and only affects the generated flow amplitudes.
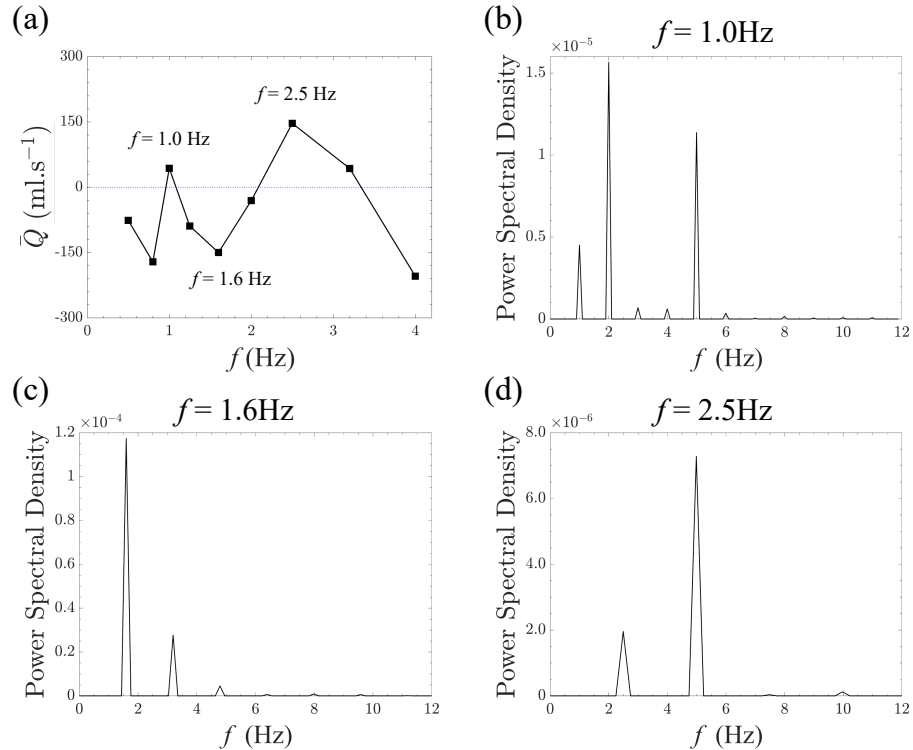
FIG. 6. Mean flow-frequency analysis at the baseline model parameters. (*a*) Mean outlet flow of the longitudinal impedance pump ($\bar{Q}$) as a function of excitation frequency. The power spectral density of the outlet flow at the frequencies of (*b*) 1Hz, (*c*) 1.6Hz, and (*d*) 2.5Hz.

E. Effect of the tube stiffness and length

Fig. 12(a) presents $\bar{Q}$ as a function of frequency for different tube stiffness (measured by wave speed)[33]. Simulations are run for four different wave speeds, starting from C_1, corresponding to the baseline parameters of the model ($r = 0.015$m, $E = 100$KPa, and thickness of 0.001m). The tube radius and wall thickness remained constant throughout this study, and only the wall elasticity is changed to alter the wave speed. Results suggest that changing the tube characteristics strongly affect the net flow generation in longitudinal impedance pump. Alteration of the wave speed affects the wave travel time and consequently changes the interactions of the propagated and reflected waves. As described earlier, the flow generation in the longitudinal impedance pump is the result of the net effect of the stretching suction and the compression waves. The alteration in the material characteristics and wave speed affect the intensity of the compression waves[15] and hence, results in a different mean flow-frequency pattern as shown in Fig. 9(a). These results suggest that at some frequencies (e.g., 3.2Hz),

for the same stretching amplitude, the flow can be either positive or negative depending on the wave speed inside the tube.

Mean flow-frequency relation as a function of the wave speed are further studied using dimensionless wave condition number (*WCN*) demonstrated in Fig. 12(b). This scaling helps investigating the behavior of longitudinal impedance pump across different range of parameters. *WCN* is a quantity that determines the state of wave dynamics in an elastic tube (computed by $WCN = fL/c$[32]) and and its applicability in the cardiovascular engineering has been shown previously using animal data, in-vitro modeling, and allometry analysis[50]. As demonstrated by this figure, the computed results at different wave speeds collapse on top of each other and the nonlinearity in mean flow-frequency pattern is well-captured using *WCN*. Hence, this scaling facilitates understanding the non-linear mean flow-frequency pattern which exists in the longitudinal impedance pump across wide range of parameters. Fig. 12(c) presents mean outlet flow $\bar{Q}$ for $SR = 0.1$ as a function of frequency for different tube lengths. Varying the tube length changes the location of the reflection site in our
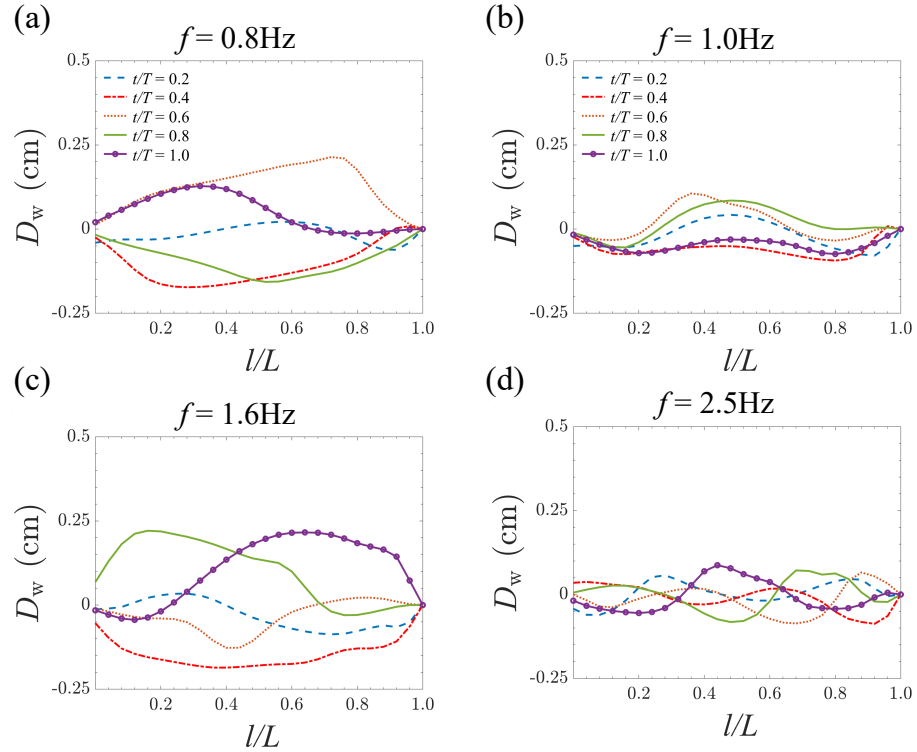
FIG. 7. Tube wall displacement as a function of frequency. Computed radial wall displacements (D_w) at different locations l along the tube length L at different snapshots in time for (a) $f = 0.8$Hz, (b) $f = 1.0$Hz, (c) $f = 1.6$Hz, and (d) $f = 2.5$Hz.

model – the end of the tube. This affects the wave interaction. Simulations are run for four lengths, starting from $L_1 = 50$cm. As the wave state changes due to the alteration in the tube length, the net effect of the suction and compression waves changes and therefore, the peaks in the mean flow-frequency pattern shift. Fig. 12(d) depicts the normalized outlet flow at each tube length as a function of *WCN*.

This study has certain limitations that should be considered. We utilized Newtonian flow assumption for the fluid in this study. This assumption is still conventionally used in both experimental and computational studies in large arteries such as aorta in the cardiovascular research[51]. However, future studies are needed to investigate the significance of non-Newtonian flow behavior in the longitudinal impedance pump. In this study, we considered one reflection site at the tube outlet. In the cardiovascular system and in major arteries such as aorta, there are multiple reflection sites. Hence, future studies can include the effect of multiple reflection sites on the longitudinal wave pumping.

IV. CONCLUSION

The present work provides a comprehensive analysis on a novel type of the impedance pump with longitudinal stretching as an excitation mechanism. By examining a wide range of parameters, the pump's nature is described and the underlying mechanism in the mean flow-frequency pattern is discussed. It was shown that the pumping characteristics in such systems is the result of the net impact of the suction, created due to the stretching, and the compression waves, created as a result of the interaction between propagating and reflected waves due to the presence of the reflection site. Like other impedance pumps, the unique frequency-dependence of the net flow rate implies an impedance-driven flow. It was shown that both the direction and amplitude of the net generated flow depend strongly on the wave dynamic characteristics including the stretching frequency, tube wall elasticity and the tube length. From the frequency spectra, it was shown that for the for the energetic mode of the tube wall, the effects of the pres-
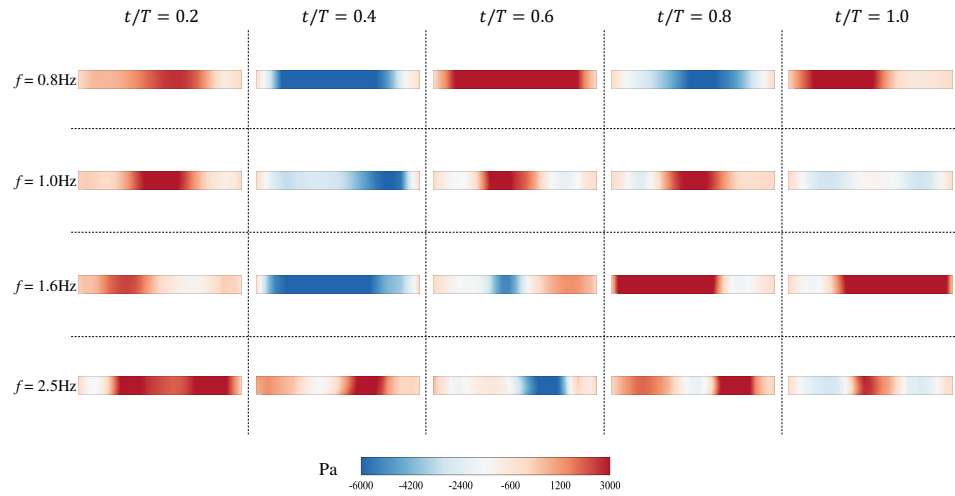
FIG. 8. Spatial distributions of flow behavior in the longitudinal impedance pump model at different snapshots of time during cycle T and for different frequencies. The plots in each row present pressure distributions. For the visualization purpose, the deflection of the wall is neglected. The tube length is the baseline value of 0.5m
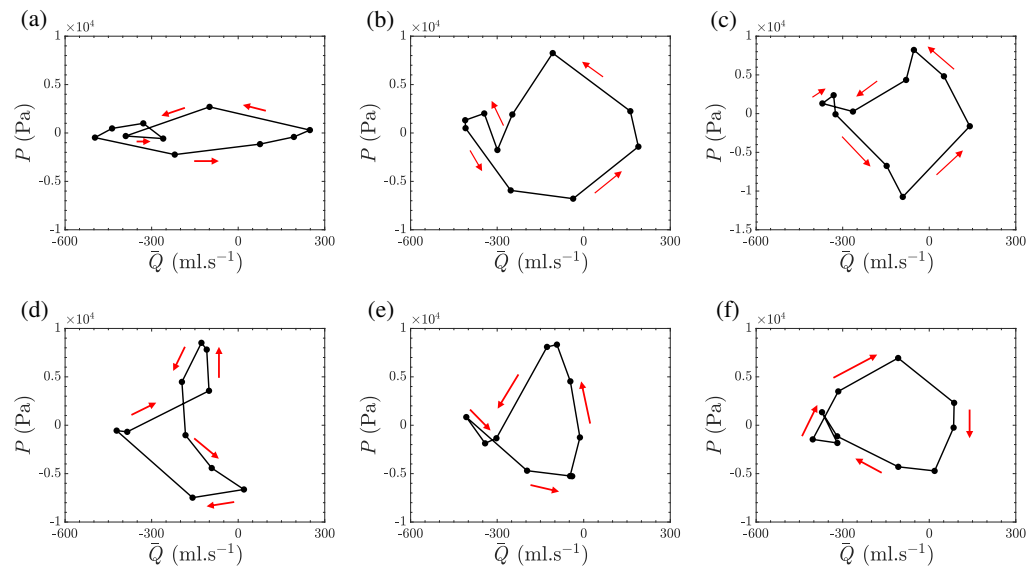

FIG. 9. Pressure-flow $(P - Q)$ loops at six locations along the tube for stretching frequency of 1.6 Hz. Arrows indicate the direction of the loop. The axial distance from the inlet (stretching site) are $(a)\, z = 2$ cm, $(b)\, z = 8$cm, $(c)\, z = 14$cm, $(d)\, z = 30$cm, $(e)\, z = 36$cm, and $(f)\, z = 42$cm.

Accepted to Phys. Fluids 10.1063/5.0165150

On the Longitudinal Wave Pumping in Fluid-filled Compliant Tubes   11
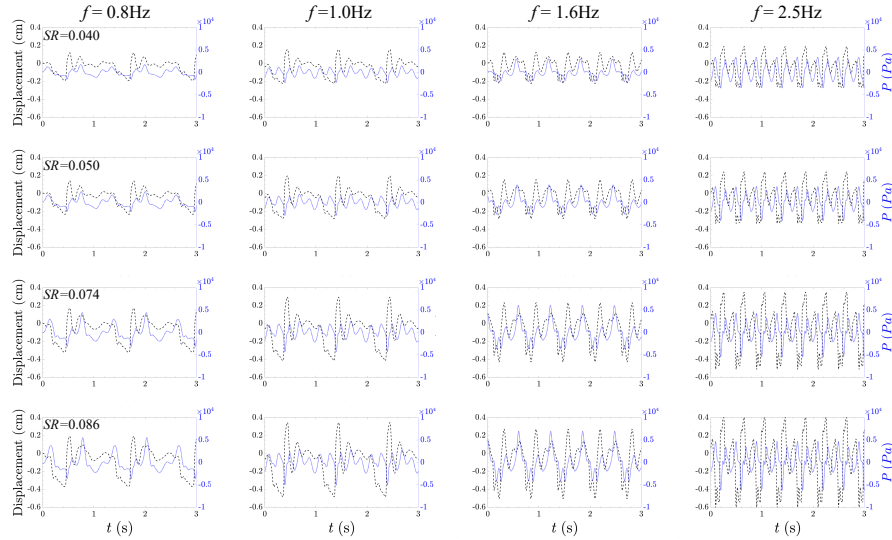
FIG. 10. Sample displacement and pressure waveforms collected 5cm away from the outlet. Data in each row is collected for the fixed stretching amplitude and in each column is collected for the fixed stretching frequency.

sure suction due to the stretching is dominant and the net generated flow is negative (reverse pumping). The transition in the tube wall displacement mode leads to the resonance-like behavior in the mean flow-frequency pattern which ultimately results in the flow pumping (positive generated flow). Our results also suggest that wave condition number can be used to capture the non-linearity in the mean flow-frequency relation across different scales. Overall, the results presented in this study offer a comprehensive investigation into the fundamental physics underlying an impedance pump with longitudinal stretching, with a particular focus on the concept of stretch-related wave pumping. These findings could also serve as a design guideline for future applications of longitudinal impedance pumps. This has potential practical implications in biomedical research, where such pumps could improve assist devices and aid in valveless flow circulation.

Appendix A: Discretization tests

To ensure independence of the results from temporal and spatial discretization, the time step Δt and total number of elements in both domains N (total number of elements) of a case are varied while keeping all other parameters unchanged. First, we performed the same computation with different time steps while keeping N at 4000 elements. The time step is increased or decreased by a factor of 2, starting at $\Delta t = 1/500f$. The time step convergence criterion was defined less than 3% change in outlet longitudinal velocity given a factor of 2 decrease in Δt. The largest time step satisfying this crite-

rion, $\Delta t = 1/1000f$, is ultimately selected. In order to consider different period lengths, the timestep is a function of the stretching frequency. Then, while keeping the time step at $\Delta t = 1/1000f$, N is incremented by $\pm 20\%$, rounded to the nearest hundred and starting at $N = 4000$. The number of the elements was maintained at 40 (fluid domain) and 10 (solid domain) along the radial direction such that changing N only changes the number of elements in the longitudinal direction (which was the same for both domains). Note that these numbers are obtained for the largest tube length used in this study (i.e., L=50cm). The spatial convergence criterion was defined as less than 3% change in outlet longitudinal velocity given a 20% change in N. The results of the study are summarized in Fig. 13 for the case with parameters of $f = 1$Hz and $SR = 0.1$.

Appendix B: Oscillatory steady-state condition

The fluid-filled elastic tube system began at rest in each simulation, then is excited until an oscillatory steady state is achieved. To track the periodicity of the fluid motion, mean outlet flow is computed by integrating the fluid velocity across the outlet elements over the duration of one period T. The oscillatory steady-state criterion is defined as less than 1% change in mean outlet flow compared to the previous cycle[52]. This is typically achieved within 35 cycles. A sample transient response of flow rate is shown in Fig. 14(a) for case parameters $f = 2.5$Hz and elasticity of 100KPa, and $SR = 0.1$. There is a transitional stage for the flow to build up before reaching its steady-state mean. Fig. 14(b) presents the tube root
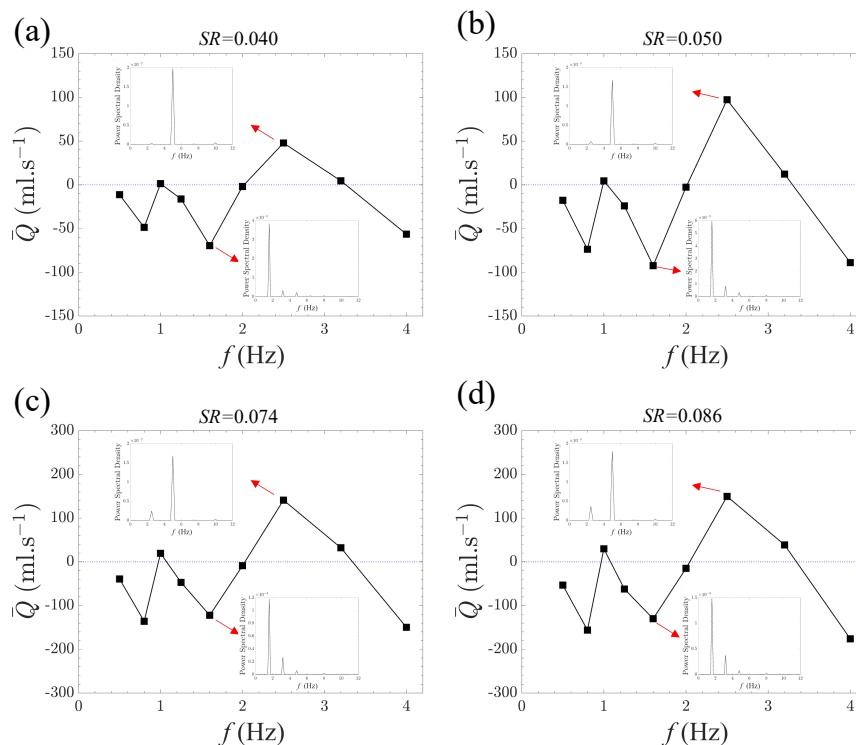
Accepted to Phys. Fluids 10.1063/5.0165150

On the Longitudinal Wave Pumping in Fluid-filled Compliant Tubes 12

FIG. 11. Mean flow-frequency analysis at different levels of the root displacements. Mean outlet flow of the longitudinal impedance pump ($\bar{Q}$) as a function of excitation frequency for stretching of (*a*) 2cm corresponding to *SR* = 0.04, (*b*) 2.5cm corresponding to *SR* = 0.05, (*c*) 3.7cm corresponding to *SR* = 0.074, and (*d*) 4.3cm corresponding to *SR* = 0.086. The power spectral density of the outlet flow at the frequencies corresponding to the peak flows are also demonstrated.

elongation for the same case.

Appendix C: Power Expenditure

Fig. 15 shows the power expenditure, computed form the loop areas of the P-Q curves, as a function of axial location along the tube for three representative frequencies. Negative areas indicate conversion of fluid energy to elastic energy, and positive areas indicate elastic energy converted to fluid energy. For each case, the loop area changes sign between the inlet (stretching zone) and outlet (reflection site). The magnitude of energy exchange along the tube is larger at the frequencies lead to the energetic mode (0.8 and 1.6Hz) compared with the frequency corresponds to the ordinary mode (1.0 Hz). These results are obtained for the baseline tube length of 0.5m.
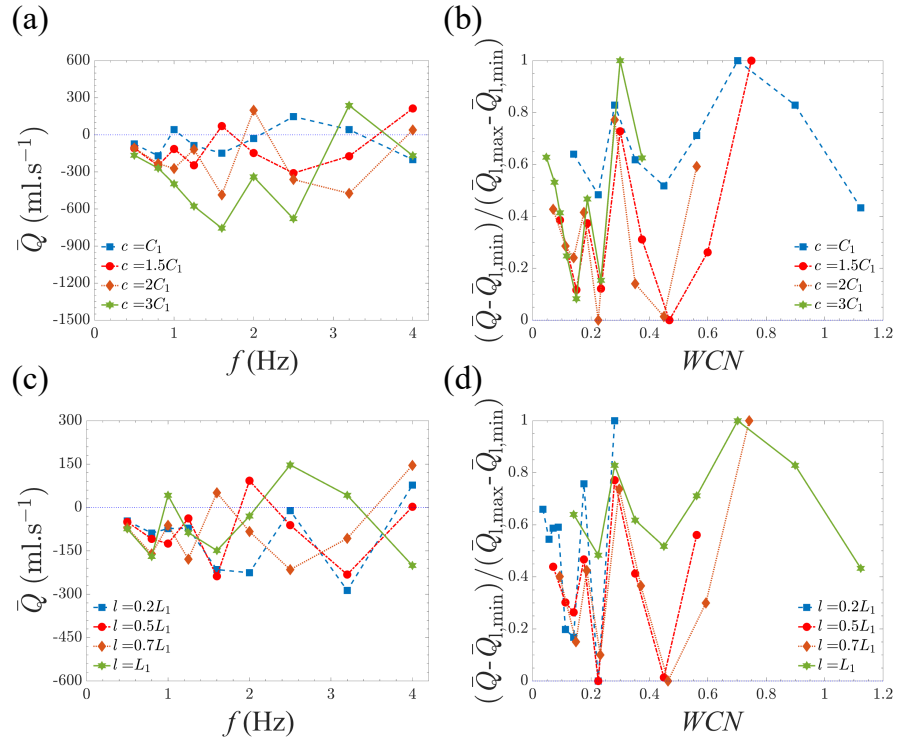
DATA AVAILABILITY STATEMENT

The data that support the findings of this study are included in the figures and the methods are provided within the body of

FIG. 12. Impact of tube stiffness and length on the generated flow in the longitudinal impedance pump. (*a*) Mean outlet flow of the longitudinal impedance pump ($\bar{Q}$) against the excitation frequency for different levels of wave speed c. (*b*) The normalized outlet flow of the longitudinal impedance pump against the wave condition number (*WCN*) for different levels of wave speed c. (*c*) Mean outlet flow as a function of excitation frequency for different tube lengths. (*d*) Normalized outlet flow as a function of wave condition number (*WCN*) for different tube length. Results are presented for the stretching ratio of 0.1

the paper.

REFERENCES

[1]C.-Y. Wen and H.-T. Chang, "Design and characterization of valveless impedance pumps," Journal of Mechanics **25**, 345–354 (2009).

[2]M. Rosenfeld and I. Avrahami, "Net flow rate generation by a multi-pincher impedance pump," Computers & Fluids **39**, 1634–1643 (2010).

[3]D. Rinderknecht, A. I. Hickerson, and M. Gharib, "A valveless micro impedance pump driven by electromagnetic actuation," Journal of Micromechanics and Microengineering **15**, 861 (2005).

[4]A. S. Forouhar, M. Liebling, A. Hickerson, A. Nasiraei-Moghaddam, H.-J. Tsai, J. R. Hove, S. E. Fraser, M. E. Dickinson, and M. Gharib, "The embryonic vertebrate heart tube is a dynamic suction pump," Science **312**, 751–753 (2006).

[5]C. Manopoulos, S. Tsangaris, and D. Mathioulakis, "Net flow generation in closed-loop valveless pumping," Proceedings of the Institution of Mechanical Engineers, Part C: Journal of Mechanical Engineering Science **234**, 2126–2142 (2020).
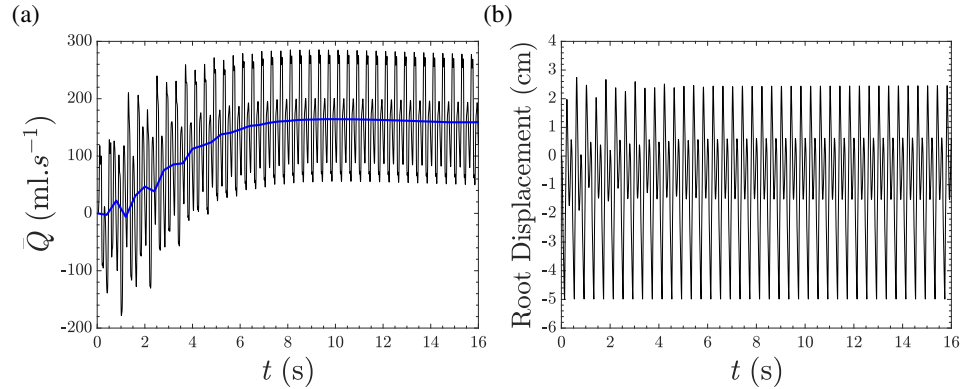
[6]A. I. Hickerson, D. Rinderknecht, and M. Gharib, "Experimental study of the behavior of a valveless impedance pump," Experiments in fluids **38**, 534–540 (2005).

[7]G. Liebau, "Über ein ventilloses pumpprinzip," Naturwissenschaften **41**, 327–327 (1954).

[8]P. Longatti, "The liebau phenomenon: a translational approach to new paradigms of csf circulation and related flow disturbances," Child's Nervous System **34**, 227–233 (2018).

[9]J. T. Ottesen, "Valveless pumping in a fluid-filled closed elastic tube-system: one-dimensional theory with experimental validation," Journal of mathematical biology **46**, 309–332 (2003).

[10]A. Borzi and G. Propst, "Numerical investigation of the liebau phenomenon," Zeitschrift für angewandte Mathematik und Physik ZAMP **54**, 1050–1072 (2003).

[11]G. Propst, "Pumping effects in models of periodically forced flow configurations," Physica D: Nonlinear Phenomena **217**, 193–201 (2006).

[12]S. Timmermann and J. T. Ottesen, "Novel characteristics of valveless pumping," Physics of Fluids **21**, 053601 (2009).

[13]C. Manopoulos, S. Tsangaris, and D. Mathioulakis, "Net flow generation in closed-loop valveless pumping," Proceedings of the Institution of Mechanical Engineers, Part C: Journal of Mechanical Engineering Science **234**,

FIG. 13. Different test cases for examining the associated error in the control parameter (the outlet axial velocity) for various (*a*) time steps and (*b*) spatial mesh.
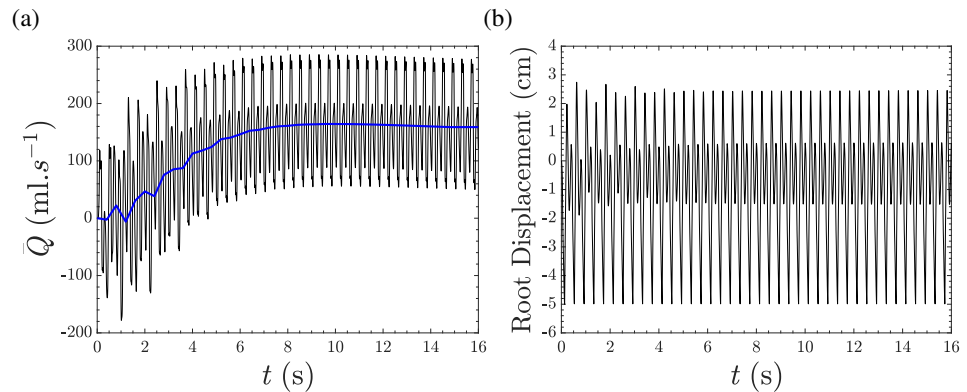

FIG. 14. Different test cases for examining the associated error in the control parameter (the outlet axial velocity) for various (*a*) time steps and (*b*) spatial mesh.

2126–2142 (2020).

[14] N. Sarvazyan, "Building valveless impedance pumps from biological components: Progress and challenges," Frontiers in physiology , 2407 (2022).

[15] N. M. Pahlevan and M. Gharib, "Pathological wave dynamics: A postulate for sudden cardiac death in athletes," Medical Hypotheses **82**, 64–70 (2014).

[16] J. Floryan, S. Panday, and K. M. Faisal, "On the peristaltic pumping," Physics of Fluids **33**, 033609 (2021).

[17] E. Jung and C. S. Peskin, "Two-dimensional simulations of valveless pumping using the immersed boundary method," SIAM Journal on Scientific Computing **23**, 19–45 (2001).

[18] A. I. Hickerson and M. Gharib, "On the resonance of a pliant tube as a mechanism for valveless pumping," Journal of Fluid Mechanics **555**, 141–148 (2006).

[19] I. Avrahami and M. Gharib, "Computational studies of resonance wave pumping in compliant tubes," Journal of Fluid Mechanics **608**, 139–160 (2008).

[20] L. Loumes, I. Avrahami, and M. Gharib, "Resonant pumping in a multilayer impedance pump," Physics of Fluids **20**, 023103 (2008).

[21] R. A. Carmigniani, M. Benoit, D. Violeau, and M. Gharib, "Resonance wave pumping with surface waves," Journal of Fluid Mechanics **811**, 1–36 (2017).

[22] J. Anatol, M. García-Díaz, C. Barrios-Collado, J. Moneo-Fernández, F. Castro-Ruiz, and J. Sierra-Pallares, "Experimental characterization of an asymmetric valveless pump based on soft robotics technology," Physics of Fluids **35** (2023).

[23] J. Anatol, M. García-Díaz, C. Barrios-Collado, J. Moneo-Fernández, M. Horvath, T. Parra, F. Castro-Ruiz, E. Roche, and J. Sierra-Pallares, "Ex-
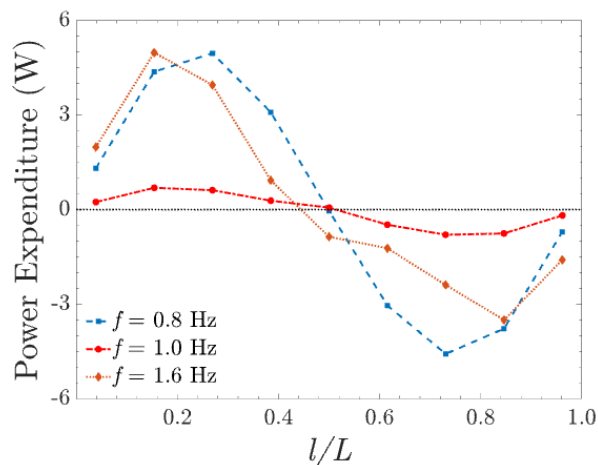
FIG. 15. Power expenditure, computed from the pressure-flow $(P - Q)$ loop areas, at different locations along the tube for three frequencies. The length of the tube is at the baseline value of 0.5m.

perimental study of an asymmetric valveless pump to elucidate insights into strategies for pediatric extravascular flow augmentation," Scientific Reports **12**, 22165 (2022).

[24]A. Sharifi, A. Gendernalik, D. Garrity, and D. Bark, "Valveless pumping behavior of the simulated embryonic heart tube as a function of contractile patterns and myocardial stiffness," Biomechanics and Modeling in Mechanobiology **20**, 2001–2012 (2021).

[25]N. M. Pahlevan and M. Gharib, "In-vitro investigation of a potential wave pumping effect in human aorta," Journal of Biomechanics **46**, 2122–2129 (2013).

[26]Z. Li, Y. Seo, O. Aydin, M. Elhebeary, R. D. Kamm, H. Kong, and M. T. A. Saif, "Biohybrid valveless pump-bot powered by engineered skeletal muscle," Proceedings of the National Academy of Sciences **116**, 1543–1548 (2019).

[27]R. Davtyan and N. A. Sarvazyan, "Output of a valveless liebau pump with biologically relevant vessel properties and compression frequencies," Scientific reports **11**, 1–9 (2021).

[28]V. Bell and G. F. Mitchell, "Influence of vascular function and pulsatile hemodynamics on cardiac function," Current hypertension reports **17**, 1–9 (2015).

[29]V. Bell, S. Sigurdsson, J. J. Westenberg, J. D. Gotal, A. A. Torjesen, T. Aspelund, L. J. Launer, T. B. Harris, V. Gudnason, and A. de Roos, "Relations between aortic stiffness and left ventricular structure and function in older participants in the age, gene/environment susceptibility-reykjavik study," Circulation: Cardiovascular Imaging **8**, e003039 (2015).

[30]P. Ballo, S. Nistri, M. Cameli, B. Papesso, F. L. Dini, M. Galderisi, A. Zuppiroli, and S. Mondillo, "Association of left ventricular longitudinal and circumferential systolic dysfunction with diastolic function in hypertension: a nonlinear analysis focused on the interplay with left ventricular geometry," Journal of cardiac failure **20**, 110–120 (2014).

[31]I. Codreanu, M. D. Robson, S. J. Golding, B. A. Jung, K. Clarke, and C. J. Holloway, "Longitudinally and circumferentially directed movements of the left ventricle studied by cardiovascular magnetic resonance phase contrast velocity mapping," Journal of Cardiovascular Magnetic Resonance **12**, 1–8 (2010).

[32]N. M. Pahlevan and M. Gharib, "A wave dynamics criterion for optimization of mammalian cardiovascular system," Journal of Biomechanics **47**, 1727–1732 (2014).

[33]A. Aghilinejad, F. Amlani, K. S. King, and N. M. Pahlevan, "Dynamic effects of aortic arch stiffening on pulsatile energy transmission to cerebral vasculature as a determinant of brain-heart coupling," Scientific reports **10**, 1–12 (2020).

[34]J. Kang, A. Aghilinejad, and N. M. Pahlevan, "On the accuracy of displacement-based wave intensity analysis: Effect of vessel wall viscoelasticity and nonlinearity," PloS one **14**, e0224390 (2019).

[35]S. Z. Pagoulatou, M. Ferraro, B. Trachet, V. Bikia, G. Rovas, L. A. Crowe, J.-P. Vallée, D. Adamopoulos, and N. Stergiopulos, "The effect of the elongation of the proximal aorta on the estimation of the aortic wall distensibility," Biomechanics and Modeling in Mechanobiology **20**, 107–119 (2021).

[36]A. Aghilinejad, H. Wei, G. A. Magee, and N. M. Pahlevan, "Model-based fluid-structure interaction approach for evaluation of thoracic endovascular aortic repair endograft length in type b aortic dissection," Frontiers in Bioengineering and Biotechnology **10** (2022).

[37]A. Arzani, A. M. Gambaruto, G. Chen, and S. C. Shadden, "Lagrangian wall shear stress structures and near-wall transport in high-schmidt-number aneurysmal flows," Journal of Fluid Mechanics **790**, 158–172 (2016).

[38]A. Arzani and S. C. Shadden, "Characterization of the transport topology in patient-specific abdominal aortic aneurysm models," Physics of Fluids **24** (2012).

[39]N. M. Pahlevan, F. Amlani, M. Hossein Gorji, F. Hussain, and M. Gharib, "A physiologically relevant, simple outflow boundary model for truncated vasculature," Annals of biomedical engineering **39**, 1470–1481 (2011).

[40]A. Aghilinejad, M. Aghaamoo, and X. Chen, "On the transport of particles/cells in high-throughput deterministic lateral displacement devices: Implications for circulating tumor cell separation," Biomicrofluidics **13** (2019).

[41]M. Aghaamoo, A. Aghilinejad, X. Chen, and J. Xu, "On the design of deterministic dielectrophoresis for continuous separation of circulating tumor cells from peripheral blood cells," Electrophoresis **40**, 1486–1493 (2019).

[42]M. Bakroon, R. Daryaei, D. Aubram, and F. Rackwitz, "Investigation of mesh improvement in multimaterial ale formulations using geotechnical benchmark problems," International Journal of Geomechanics **20**, 04020114 (2020).

[43]A. M. Bavo, G. Rocatello, F. Iannaccone, J. Degroote, J. Vierendeels, and P. Segers, "Fluid-structure interaction simulation of prosthetic aortic valves: comparison between immersed boundary and arbitrary lagrangian-eulerian techniques for the mesh representation," PloS one **11**, e0154517 (2016).

[44]R. Alavi, A. Aghilinejad, H. Wei, S. Niroumandi, S. Wieman, and N. M. Pahlevan, "A coupled atrioventricular-aortic setup for in-vitro hemodynamic study of the systemic circulation: Design, fabrication, and physiological relevancy," Plos one **17**, e0267765 (2022).

[45]T. Plonek, M. Berezowski, J. Kurcz, P. Podgorski, M. Sąsiadek, B. Rylski, A. Mysiak, and M. Jasinski, "The evaluation of the aortic annulus displacement during cardiac cycle using magnetic resonance imaging," BMC Cardiovascular Disorders **18**, 1–6 (2018).

[46]N. M. Pahlevan and M. Gharib, "Aortic wave dynamics and its influence on left ventricular workload," PloS one **6**, e23106 (2011).

[47]J. Chirinos and P. Segers, "Measurements and basic principles of wave conduction and reflection noninvasive evaluation of left ventricular afterload: part 1: pressure and flow hypertension," Hypertension **56**, 555–562 (2010).

[48]B. Kim, W.-X. Huang, S. J. Shin, and H. J. Sung, "Flexible ring flapping in a uniform flow," Journal of fluid mechanics **707**, 129–149 (2012).

[49]H. Ye, H. Wei, H. Huang, and X.-y. Lu, "Two tandem flexible loops in a viscous flow," Physics of Fluids **29**, 021902 (2017).

[50]N. M. Pahlevan and S. P. Mazandarani, "Estimation of wave condition number from pressure waveform alone and its changes with advancing age in healthy women and men," Frontiers in Physiology **11**, 313 (2020).

[51]A. Iskander, C. Bilgi, R. Naftalovich, I. Hacihaliloglu, T. Berkman, D. Naftalovich, and N. Pahlevan, "The rheology of the carotid sinus: A path toward bioinspired intervention," Frontiers in Bioengineering and Biotechnology **9**, 678048 (2021).

[52]A. Aghilinejad, R. Alavi, B. Rogers, F. Amlani, and N. M. Pahlevan, "Effects of vessel wall mechanics on non-invasive evaluation of cardiovascular intrinsic frequencies," Journal of Biomechanics **129**, 110852 (2021).